

# RESFM: Robust Equivariant Multiview Structure from Motion

Fadi Khatib<sup>1</sup>, Yoni Kasten<sup>2</sup>, Dror Moran<sup>1</sup>, Meirav Galun<sup>1</sup>, and Ronen Basri<sup>1</sup>

<sup>1</sup> Weizmann Institute of Science

<sup>2</sup> NVIDIA Research

Project webpage: [robust-equivariant-sfm.github.io](https://robust-equivariant-sfm.github.io)

**Abstract.** Multiview Structure from Motion is a fundamental and challenging computer vision problem. A recent deep-based approach was proposed utilizing matrix equivariant architectures for the simultaneous recovery of camera pose and 3D scene structure from large image collections. This work however made the unrealistic assumption that the point tracks given as input are clean of outliers. Here we propose an architecture suited to dealing with outliers by adding an inlier/outlier classifying module that respects the model equivariance and by adding a robust bundle adjustment step. Experiments demonstrate that our method can be successfully applied in realistic settings that include large image collections and point tracks extracted with common heuristics and include many outliers.

**Keywords:** 3D Reconstruction · Outlier Removal · Structure from Motion

## 1 Introduction

Simultaneous recovery of camera pose and 3D structure from large image sets, commonly termed Multiview Structure from Motion (SfM), is a longstanding fundamental problem in computer vision with applications in augmented and virtual reality, robot manipulation, and more. Classical SfM techniques as well as some recent deep-based techniques rely on the extraction of point tracks, i.e., point matches across multiple frames, to solve for camera poses and structure. Existing heuristics for point track extraction, however, often return erroneous (*outlier*) point tracks, due to large viewpoint and illumination differences and the presence of repetitive scene structures. Moreover, producing point tracks by connecting chains of pairwise matches further introduces outliers. Identifying these outlier track points significantly slows reconstruction down and in certain cases results in inaccurate reconstruction. Developing robust techniques that can efficiently and accurately remove outlier track points is still an outstanding challenge.

Early classical SfM techniques rely on point feature extraction and matching, e.g., using SIFT [21], to construct point tracks. Sequential algorithms [1, 30]

then incrementally update their camera poses and 3D sparse (point cloud) reconstruction by processing one camera at a time, pruning the outlier matches at every step of the algorithm. While such processing, often yields state-of-the-art results, it can be slow, particularly for large image collections.

Recent deep-based methods attracted considerable attention due to their ability to encode priors for cameras and shapes effectively. In particular, Neural Radiance Field (NeRF) methods and methods based on implicit surface reconstruction exploit such priors to obtain accurate dense (pixel resolution) reconstruction [6, 24, 39, 40]. Yet, many of these methods still rely on classical methods to estimate camera pose. Moreover, deep methods for multiview SfM (see review in Section 2) are typically applied to small image collections, usually  $\leq 20$  images [36], due to both accuracy and complexity considerations. The problem of using deep networks in large multiview SFM setups, even in the sparse setting, is still unsolved.

Below we introduce a robust, deep-based technique for multiview SfM. We address multiview SfM in its classical setting and modify and extend the recent method of Moran et al. [23] to filter out outlier track points. Moran et al. obtain a collection of point tracks as input, which they arrange in the columns of a matrix (tensor) whose rows represent the cameras. Their work, which is inspired by projective factorization techniques, uses a network that is equivariant to both matrix row and column permutations [10] to map the point tracks to camera poses and 3D structures. Their method, however, only works on inputs in which all outliers are removed in preprocessing. This severely limits the applicability of their method.

In this paper, we extend the approach presented in [23], by adding an inlier/outlier classification module that respects equivariance. In particular, our architecture allows identifying track points that behave inconsistently compared to other points of the same image (i.e., points that share the same matrix row) or are inconsistent with other members of their track (i.e., sharing the same column). Additionally, we modify the final bundle adjustment step to make it robust to classification errors. These modifications allow our model to (1) handle large image collections (hundreds of images) of novel scenes not seen in training, and (2) use point tracks obtained with standard common heuristics that include many outliers without any pre-filtering of these outliers. Experiments show that our network improves over the method of [23] in almost all runs, obtaining state-of-the-art accuracies while considerably reducing run time, compared to the classical COLMAP [12].

## 2 Related Work

The recovery of camera pose and 3D structure from image collections has been a central subject of research in computer vision in the past several decades, leading to multiple breakthroughs that enabled accurate reconstructions from hundreds and even thousands of unordered images [1, 25, 30, 32, 38]. In the typical *sequential*

*pipeline* point tracks are first extracted from the input images. Camera pose and 3D structure are next computed for two images and then updated by processing the remaining images one by one. This pipeline yields highly accurate recovery of pose and structure but can be slow when applied to large image collections. Alternative global approaches attempt to solve SfM simultaneously for all images using a variety of factorization formulations [13, 22, 33].

Recent deep-learning techniques attempt to improve these pipelines by exploiting the priors on the input images, camera settings and 3D structures learned with these networks. Existing methods attempt to improve keypoint detection and matching [8, 19, 20, 29, 34], produce point tracks [11] formulate differentiable alternatives to RANSAC [35, 41, 44, 45], or directly infer the relative orientation and location of a pair of images [3, 5, 14, 16, 28].

Recent work proposed end-to-end methods for camera pose estimation. Works such as RelPose [43] and its successor, RelPose++ [18], harness energy-based models to recover camera poses from input that includes the relative rotations between images. Similarly, SparsePose [31] learns to regress initial camera poses which are then refined iteratively. PoseDiffusion [36] employs a diffusion model to refine camera poses. [42] improve this by focusing on purifying the camera rays. These works, however, are only applied to small collections of images (typically  $\leq 20$ ) and are commonly applied in object-centric scenarios, e.g., as in [27].

Our approach extends the work of [23], which introduced a trainable network for simultaneous camera pose and 3D structure recovery. This approach was demonstrated to achieve highly accurate pose and structure recovery on large image collections (with several hundreds of images) of outdoor urban scenes. It however requires point tracks as input in which all outliers are removed in preprocessing. This greatly restricts its applicability in realistic settings.

[23] adopts a methodology motivated by projective factorization schemes. Arranging the input point tracks in a matrix, an equivariant network to row and column permutations is used to regress the camera poses and the 3D point cloud coordinates. The network is trained with unsupervised data by optimizing a reprojection loss and is applied at inference to novel scenes not seen in training. Additional fine-tuning and Bundle Adjustment (BA) are applied to attain sub-pixel reprojection errors. We improve over this work by adding an inlier/outlier classification module that respects and exploits the equivariant structure of the network and by introducing a robust BA scheme, allowing us to work with realistic point tracks that are obtained with standard heuristics.

We finally mention two concurrent extensions of [23] published in Arxiv. [4] replace the set of sets architecture in [23] with a graph attention network, for increased expressiveness, enabling them to avoid fine-tuning, thereby reducing inference runtime compared to [23] without compromising the performance. In [7] applied [23]’s network (with some modifications) to aerial images captured with GPS information under roughly constant camera orientation. Neither [4, 7] show results on point tracks contaminated by a significant number of outliers.

### 3 Method

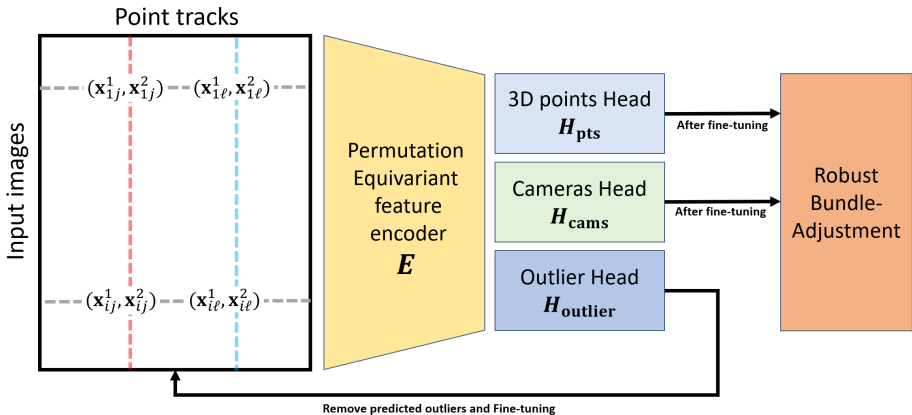


**Fig. 1: Network architecture.** Our network comprises three main modules and works in these stages (1)  $E$ , the feature encoder, which outputs a latent feature representation; (2) a module that removes predicted outliers from the input point tracks; (3) a process where the network is fine-tuned for 1000 epochs; and (4) a final stage where the predicted cameras and point cloud are optimized by bundle adjustment (BA), resulting in optimized cameras and 3D points.

Our goal is to utilize deep networks for robust multiview Structure from Motion. Given a collection of point tracks extracted from input images, we aim to simultaneously recover the unknown camera poses and the (sparse) 3D scene structure. We follow and modify the approach suggested in [23] and aim to use matrix row and column permutation equivariant network to solve the problem. As existing matching heuristics generally produce many outliers, we learn to classify track points as either inliers or outliers while relying on the sets-of-sets equivariant structure suggested in [23].

#### 3.1 Problem formulation

We assume a stationary scene viewed by  $m$  cameras with unknown poses, and we obtain as input a (sparse) point track tensor  $M$ , which includes the 2D observations of  $n$  3D points viewed by partial sets of cameras. We further assume in this work that the cameras are internally calibrated. A camera matrix therefore is expressed in the form of  $P_i = [R_i | \mathbf{t}_i]$  where  $R_i \in SO(3)$  is a rotation matrix. With this notation, the camera is placed at the position  $-R_i^T \mathbf{t}_i$ . We denote by  $\mathbf{X}_j$  the  $j$ 'th 3D scene point and by  $\mathbf{x}_{ij} \in \mathbb{R}^2$  its observed position in the  $i$ 'th image. The set  $T_j = \{\mathbf{x}_{i_1j}, \mathbf{x}_{i_2j}, \dots\}$  with  $C_j = \{i_1, i_2, \dots\} \subseteq [m]$  represents the  $j$ 'th track. These tracks are constructed in preprocessing by a heuristic and therefore are contaminated by small displacement errors and outliers.

We arrange the tracks  $T_1, \dots, T_n$  in the columns of the measurement point track tensor  $M$ . The tensor  $M$  is of size  $m \times n \times 2$ , so the rows of  $M$  correspond to the  $m$  cameras, and its columns correspond to the unknown 3D points whose contaminated projections are given. We further set  $(M_{ij1}, M_{ij2}) = \mathbf{x}_{ij}$  if  $i \in C_j$  and  $C_j$  represents the set of images in which  $X_j$  is detected. Otherwise,  $M_{ij1}$  and  $M_{ij2}$  are empty.

We aim to recover the pose parameters of the  $m$  camera matrices and the 3D positions of the  $n$  feature points. Additionally, we seek to classify each track point as either an inlier or an outlier. The output of our network will comprise three matrices:  $P \in \mathbb{R}^{m \times 7}$  for the set of cameras matrices,  $X \in \mathbb{R}^{n \times 3}$  for the 3D structure, and  $O \in \mathbb{R}^{m \times n}$  for the track point classification results. Here every camera in  $P$  is represented by a rotation quaternion  $\mathbf{q}_i \in \mathbb{R}^4$  and a translation vector  $\mathbf{t}_i \in \mathbb{R}^3$ . Classification results in  $O$  are represented by scores in  $[0, 1]$ , where  $\tilde{\mathbf{x}}_{ij}$  with  $O_{ij} \geq 0.6$  is considered an outlier.

### 3.2 Network architecture

Our architecture is equivariant to both row and column permutations of  $M$ , as in [23]. It comprises four modules (see Fig. 1): an equivariant feature encoder followed by an outlier removal, pose, and structure prediction modules.

**Equivariant feature encoder.** This module takes as input the tensor  $M \in \mathbb{R}^{m \times n \times 2}$  and outputs a latent representation in  $\mathbb{R}^{m \times n \times d}$ , where  $d = 256$ . It comprises 3 permutation equivariant layers interspersed with pointwise non-linear ReLU function, to process and encode the features.

**An equivariant layer.** A linear equivariant map is the core of permutation equivariant networks. In our case, the permutation equivariance should hold on rows (cameras) and columns (3D points) of the tensor  $M$ . In [10], it was shown that the space of linear maps that keep the permutation equivariant property of a single channel (i.e., the input and the output are matrices) is spanned by the identity, the row sums, the column sums, and the matrix sum. In [23], it was applied to multiple input and output channels from a feature space with  $d$  channels  $\mathbb{R}^{m \times n \times d}$  to a feature space with  $d'$  channels  $\mathbb{R}^{m \times n \times d'}$  in the following way:

$$L(\tilde{M})_{ij} = W_1 \tilde{M}_{ij} + W_2 \sum_{k=1}^m \tilde{M}_{kj} + W_3 \sum_{l=1}^n \tilde{M}_{il} + W_4 \sum_{k=1}^m \sum_{l=1}^n \tilde{M}_{kl} + \mathbf{b}, \quad (1)$$

where for the input tensor  $\tilde{M}_{ij}$  is a vector in  $\mathbb{R}^d$ ,  $W_i \in \mathbb{R}^{d' \times d}$  for  $i = 1, \dots, 4$ , and  $\mathbf{b} \in \mathbb{R}^{d'}$  are learnable parameters. We follow [23] and replace sums by averages over the non-empty entries of  $M$ , yielding invariance to unobserved projections.

**Inlier/Outlier classification module.** Given the latent representation  $\mathbb{R}^{m \times n \times d}$  provided by the equivariant feature encoder, this module,  $H_{\text{outlier}}$ , employs 3

MLP layers followed by a sigmoid function. The output is a matrix  $O \in [0, 1]^{m \times n}$  expressing the probability of each entry being an outlier. Note that this module respects the equivariance property.

**Pose and structure regression modules.** Utilizing the latent representation  $\mathbb{R}^{m \times n \times d}$  from the equivariant feature encoder, the pose and structure heads,  $H_{\text{cams}}$  and  $H_{\text{pts}}$ , consist of 3 MLP layers each. The first,  $H_{\text{cams}}$ , processes the pooled average of the features along the columns  $\mathbb{R}^{m \times d}$ , where each camera’s features are encoded into a vector in  $\mathbb{R}^d$ , and outputs a tensor in  $\mathbb{R}^{m \times 7}$ . This tensor encapsulates the camera’s translation vector (first three values) and orientation (last four values, represented as a quaternion), collectively forming the camera’s projection matrix. The second head,  $H_{\text{pts}}$ , processes the pooled average of features along the rows  $\mathbb{R}^{n \times d}$ , where each scene point is encoded into a vector in  $\mathbb{R}^d$ , and outputs a tensor in  $\mathbb{R}^{n \times 3}$ , representing the coordinates of the scene points.

### 3.3 Inference

After training our network (see Section 4 for details), we test the network on unseen scenes. We first apply inference and then use fine-tuning followed by robust Bundle Adjustment.

**Fine-tuning.** At this step, we leverage our inlier/outlier classification prediction and remove the points predicted as outliers from the point tracks tensor  $M$  (using the threshold 0.6). Subsequently, similar to [23], we fine-tune the network by minimizing the unsupervised reprojection loss for 1000 epochs.

**Robust Bundle Adjustment.** As common in SfM pipelines, a post-processing step of applying bundle adjustment is necessary to achieve sub-pixel reconstruction accuracy. [23] proposed first applying bundle adjustment to the predicted cameras and 3D point cloud. Next, they use the optimized camera poses from the previous step to triangulate the scene’s point cloud and subsequently reapply bundle adjustment. However, this approach was found to be non-robust in realistic scenarios involving many outliers. Therefore, propose a Robust Bundle Adjustment Module:

1. Apply bundle adjustment (BA) to the predicted cameras and predicted 3D points.
2. Remove 3D points with projection error higher than 5 pixels and remove 3D points viewed in fewer than 3 cameras.
3. If the view graph of the point tracks becomes unconnected due to the removals, then we take the largest component and discard point tracks from the removed images.
4. Triangulate the remaining point tracks and apply a second round of (standard) BA.
5. Bring back the point tracks removed in step 2, triangulate them with the optimized camera poses, and apply a third and final round of BA. This step succeeds in restoring many of the 3D points.

More details on the BA stage can be found in the appendix.

### 3.4 Loss Function

Our loss function combines two terms:

$$\mathcal{L} = \mathcal{L}_{\text{outliers}} + \alpha \mathcal{L}_{\text{reprojection}} \quad (2)$$

where the hyperparameter  $\alpha$  balances the two terms. The outlier classification loss,  $\mathcal{L}_{\text{outliers}}$ , employs a Binary Cross-Entropy (BCE) loss.  $\mathcal{L}_{\text{reprojection}}$ , which is adopted from [23], includes a reprojection and a hinge loss terms. The reprojection loss aims to minimize the error between projected scene points and their detected positions in the image, akin to the objective in bundle adjustment. Additionally, a hinge loss is used to prevent the prediction of non-positive depth values, thus ensuring a physically plausible scene reconstruction.

$$\mathcal{L}_{\text{reprojection}} = \frac{1}{p} \sum_{i=1}^m \sum_{j=1}^n \xi_{ij} s_{ij}, \quad (3)$$

Where  $p = \sum_{j=1}^n |T_j|$  the number of measured projections, and  $\xi_{ij} \in \{0, 1\}$  is indicating whether point  $\mathbf{X}_j$  is detected in image  $I_i$ .

$$s_{ij} = \begin{cases} r_{ij}, & P_i^3 \mathbf{X}_j \geq h \\ h_{ij}, & P_i^3 \mathbf{X}_j < h, \end{cases}$$

And

$$r_{ij} = \left\| \left( \mathbf{x}_{ij}^1 - \frac{P_i^1 \mathbf{X}_j}{P_i^3 \mathbf{X}_j}, \mathbf{x}_{ij}^2 - \frac{P_i^2 \mathbf{X}_j}{P_i^3 \mathbf{X}_j} \right) \right\|,$$

And  $h_{ij} = \max(0, h - P_i^3 \mathbf{X}_j)$ , where  $h > 0$  is a small constant (in our setting,  $h = 0.0001$ ).  $h_{ij}$  therefore is the hinge loss for the depth value of  $\mathbf{X}_j$  in image  $I_i$ .

## 4 Experiments

### 4.1 Datasets

Our network is trained on scenes from the MegaDepth dataset [17] and tested on novel scenes from the MegaDepth dataset as well as the 1DSfM dataset [37]. These datasets offer a diverse range of real-world scenes, which are instrumental in assessing the robustness and versatility of our proposed architecture across different environments and challenges.

The point tracks, which our networks take as input, are constructed by concatenating pairwise matches between images within each scene. These matches are obtained by applying RANSAC to SIFT matches, ensuring a robust selection of correspondences by mitigating the influence of outliers. The detailed procedure for constructing these point tracks, including parameter settings and algorithmic choices, is provided in the appendix.

**MegaDepth.** The MegaDepth dataset [17] comprises 196 different outdoor scenes, each populated with internet photos showcasing popular landmarks around the globe. To facilitate a comprehensive evaluation, we divide the dataset into two groups based on the number of images per scene: (1) scenes with fewer than 1000 images, and (2) scenes with more than 1000 images. From the first group, we randomly sampled 27 scenes to serve as our training dataset, along with four scenes designated for validation purposes. For the test set, we randomly selected 14 scenes from the first group. Moreover, from each scene in the second group, we randomly sampled images to represent a condensed version of the scene. These samples form a part of the test dataset, introducing a significant challenge for Structure from Motion (SfM) methods due to the reduced number of images representing vast and complex scenes. In tables 2 to 3, scenes above the middle rule belong to Group 1 with fewer than 1000 images, while scenes below belong to Group 2, from which we subsampled 300 images for the test set.

**1DSFM.** The 1DSFM dataset [37] is renowned for its collection of diverse scenes reconstructed from community photo collections. It includes a variety of urban locations, making it a valuable resource for evaluating Structure from Motion (SfM) and multi-view stereo algorithms. For our purposes, the dataset offers a challenging yet realistic setting to assess our architecture’s effectiveness in dealing with large-scale reconstructions.

## 4.2 Baselines

**COLMAP [30].** Recognized as the state-of-the-art incremental Structure from Motion (SfM) method, COLMAP stands as one of the most popular solutions in the field. It demonstrates robust performance in reconstructing 3D models from unordered image collections. Notably, we utilize COLMAP to establish ground truth camera poses for the scenes in our datasets by applying it directly to the scene images. To evaluate the performance of our approach relative to COLMAP, we compare the results obtained from COLMAP with those achieved using the point tracks generated by our preprocessing stage.

**ESFM [23].** We compare our approach to the original equivariant SfM method [23] where for fairness we replace BA with our robust BA. We conduct two distinct evaluations: one in which ESFM is trained and tested on the original point tracks, which are contaminated with outliers (denoted as *ESFM*), and another where it is trained and tested on outlier-free point tracks (denoted as *ESFM\**). By comparing ESFM on the original, contaminated tracks we demonstrate our method’s ability to handle realistic settings. Comparison to the clean tracks provides an empirical upper bound for our method.

## 4.3 Metrics and Evaluation

We measure accuracy with the average reprojection error, measured in pixels as follows

$$\frac{1}{p} \sum_{i=1}^m \sum_{j=1}^n \xi_{ij} \left\| \left( \mathbf{x}_{ij}^1 - \frac{P_i^1 \mathbf{X}_j}{P_i^3 \mathbf{X}_j}, \mathbf{x}_{ij}^2 - \frac{P_i^2 \mathbf{X}_j}{P_i^3 \mathbf{X}_j} \right) \right\|.$$

For notation see Sec. 3.4. We further evaluate our predictions of camera parameters. Specifically, we compare our camera orientation predictions with the ground truth ones by measuring angular differences in degrees. Similarly, we measure differences between our predicted and ground truth camera locations (up to a global scale for the scene). For a fair comparison, both our method and all the baseline methods were run with the same set of point tracks. For all methods, we apply a final post-processing step of our robust bundle adjustment. When highlighting the best result in the tables, for a fair comparison, we only compare to ESFM.

Scene	$N_c$	Outliers%	Ours			ESFM			ESFM*			Colmap		
			$N_r$	Mean	Median	$N_r$	Mean	Median	$N_r$	Mean	Median	$N_r$	Mean	Median
0205	910	51.8	<b>386</b>	<b>2.58</b>	<b>0.509</b>	70	4.613	2.001	633	11.145	3.423	782	0.157	0.071
0238	522	44.6	<b>283</b>	<b>2.607</b>	<b>0.717</b>	76	11.494	1.751	512	3.059	0.64	515	0.307	0.096
0060	528	41.6	<b>503</b>	<b>0.286</b>	<b>0.143</b>	303	14.925	8.543	524	0.024	0.016	525	0.05	0.023
0197	870	40.7	<b>667</b>	<b>4.216</b>	<b>2.056</b>	281	9.621	4.14	825	0.412	0.111	847	0.174	0.052
0094	763	40.1	<b>537</b>	<b>3.774</b>	<b>0.382</b>	93	14.906	17.618	643	4.549	0.184	743	0.597	0.19
0265	571	38.8	<b>346</b>	<b>1.254</b>	<b>0.74</b>	270	22.143	14.641	559	0.117	0.062	560	0.316	0.145
0083	635	31.3	<b>596</b>	<b>0.642</b>	<b>0.147</b>	568	4.403	0.899	556	21.022	16.03	633	0.057	0.029
0076	558	30.5	<b>524</b>	<b>0.373</b>	<b>0.109</b>	454	3.857	1.604	547	0.043	0.03	550	0.083	0.042
0185	368	30	<b>350</b>	<b>0.063</b>	<b>0.041</b>	261	1.757	0.532	130	38.491	29.391	367	0.081	0.039
0048	512	24.2	<b>474</b>	4.689	2.157	469	<b>4.027</b>	<b>1.567</b>	508	0.091	0.046	507	0.089	0.041
0024	356	23	<b>309</b>	<b>2.032</b>	<b>0.582</b>	271	9.079	4.64	343	2.777	1.409	351	0.093	0.057
0223	214	17	<b>204</b>	<b>3.76</b>	<b>1.563</b>	191	11.973	1.811	211	0.086	0.06	214	2.546	0.409
5016	28	16.9	<b>28</b>	4.46	3.018	<b>28</b>	<b>0.092</b>	<b>0.066</b>	28	0.04	0.024	28	0.08	0.051
0046	440	14.6	<b>399</b>	<b>0.946</b>	0.785	97	1.684	<b>0.576</b>	33	37.089	29.176	440	0.013	0.007
0099	299	47.4	<b>190</b>	<b>3.529</b>	3.182	104	4.172	<b>2.212</b>	243	6.218	2.97	278	0.111	0.043
1001	285	43.9	<b>251</b>	<b>1.703</b>	<b>1.41</b>	241	4.405	2.44	280	0.121	0.084	284	7.474	6.269
0231	296	42.2	<b>246</b>	<b>0.837</b>	0.379	214	0.854	<b>0.282</b>	284	0.562	0.257	290	0.355	0.1
0411	299	29.9	<b>273</b>	<b>0.128</b>	<b>0.068</b>	188	15.886	6.21	288	0.077	0.048	290	0.171	0.099
0377	295	27.5	<b>210</b>	<b>0.287</b>	0.278	162	0.541	<b>0.249</b>	279	1.187	0.518	288	0.313	0.141
0102	299	25.8	<b>284</b>	<b>0.276</b>	<b>0.071</b>	255	1.552	0.501	155	20.996	13.565	267	0.064	0.027
0147	298	24.6	<b>207</b>	<b>4.625</b>	2.068	197	4.897	<b>2.054</b>	251	3.219	1.143	295	2.737	0.485
0148	287	24.6	197	<b>0.598</b>	<b>0.542</b>	<b>206</b>	1.644	0.592	249	0.935	0.462	277	19.61	7.418
0446	298	22.1	<b>288</b>	<b>0.715</b>	<b>0.412</b>	283	2.021	0.695	294	0.917	0.217	298	0.146	0.074
0022	297	21.2	<b>274</b>	<b>0.293</b>	<b>0.128</b>	241	1.384	0.507	289	0.302	0.085	290	0.114	0.063
0327	298	21	271	<b>0.264</b>	<b>0.112</b>	<b>281</b>	1.833	0.752	294	0.058	0.032	295	5.435	2.178
0015	284	20.6	<b>215</b>	<b>1.037</b>	<b>0.273</b>	142	4.996	1.297	185	4.514	0.432	282	0.302	0.089
0455	298	19.8	<b>293</b>	<b>0.675</b>	<b>0.183</b>	<b>293</b>	0.68	0.232	298	0.889	0.258	298	0.328	0.143
0496	297	19.2	<b>281</b>	<b>0.35</b>	<b>0.131</b>	<b>281</b>	3.586	2.806	293	0.292	0.227	295	0.263	0.124
1589	299	17.4	<b>290</b>	<b>0.145</b>	<b>0.08</b>	284	0.925	0.405	296	0.398	0.199	299	0.031	0.019
0012	299	16.3	287	<b>0.401</b>	<b>0.39</b>	<b>291</b>	5.199	2.036	294	0.471	0.224	295	0.513	0.204
0104	284	16.2	193	<b>0.29</b>	<b>0.156</b>	<b>220</b>	24.405	11.314	200	0.782	0.49	283	1.506	0.861
0019	299	15.4	250	<b>0.056</b>	<b>0.041</b>	<b>267</b>	9.339	2.463	296	4.9	2.234	298	0.031	0.018
0063	293	14.5	<b>262</b>	<b>0.462</b>	<b>0.258</b>	<b>262</b>	2.152	1.176	275	0.316	0.149	292	0.132	0.057
0130	285	14.4	<b>192</b>	<b>0.198</b>	<b>0.102</b>	<b>192</b>	1.462	0.935	282	1.589	0.82	285	1.064	0.442
0080	284	12.9	<b>139</b>	<b>0.59</b>	<b>0.266</b>	137	1.338	0.319	163	1.923	0.322	283	10.649	9.229
0240	298	11.9	<b>275</b>	3.134	1.561	274	<b>1.69</b>	<b>1.142</b>	296	0.27	0.092	298	0.115	0.058
0007	290	11.7	172	<b>0.911</b>	<b>0.234</b>	<b>260</b>	38.743	25.498	286	1.593	0.958	290	0.122	0.053

**Table 1:** MegaDepth experiment. The table shows the mean and median camera rotation error (degrees). (Above the middle rule are Group 1 scenes with <1000 images; below are Group 2 scenes with >1000 images, subsampled to 300 for testing.)

Scene	$N_c$	Outliers%	Ours			ESFM			ESFM*			Colmap		
			$N_r$	Mean	Median	$N_r$	Mean	Median	$N_r$	Mean	Median	$N_r$	Mean	Median
0205	910	51.8	<b>386</b>	<b>0.388</b>	<b>0.032</b>	70	0.702	0.328	633	1.383	0.267	782	0.029	0.01
0238	522	44.6	<b>283</b>	<b>0.448</b>	<b>0.043</b>	76	1.088	0.1	512	0.142	0.038	515	0.068	0.011
0060	528	41.6	<b>503</b>	<b>0.035</b>	<b>0.011</b>	303	2.167	1.268	524	0.005	0.003	525	0.009	0.004
0197	870	40.7	<b>667</b>	<b>0.346</b>	<b>0.133</b>	281	0.989	0.183	825	0.071	0.008	847	0.024	0.005
0094	763	40.1	<b>537</b>	<b>0.754</b>	<b>0.015</b>	93	1.772	2.048	643	1.068	0.014	743	0.065	0.015
0265	571	38.8	<b>346</b>	<b>0.389</b>	<b>0.209</b>	270	2.696	1.666	559	0.039	0.022	560	0.109	0.04
0083	635	31.3	<b>596</b>	<b>0.059</b>	<b>0.009</b>	568	0.577	0.027	556	1.907	0.973	633	0.007	0.002
0076	558	30.5	<b>524</b>	<b>0.094</b>	<b>0.01</b>	454	0.666	0.091	547	0.006	0.004	550	0.013	0.006
0185	368	30	<b>350</b>	<b>0.019</b>	<b>0.006</b>	261	0.31	0.037	130	2.481	2.16	367	0.012	0.004
0048	512	24.2	<b>474</b>	<b>0.179</b>	0.098	469	0.276	<b>0.08</b>	508	0.006	0.002	507	0.01	0.003
0024	356	23	<b>309</b>	<b>0.458</b>	<b>0.046</b>	271	1.401	0.187	343	0.571	0.078	351	0.025	0.015
0223	214	17	<b>204</b>	<b>0.511</b>	<b>0.078</b>	191	2.496	0.18	211	0.017	0.01	214	0.162	0.025
5016	28	16.9	<b>28</b>	0.974	0.179	<b>28</b>	<b>0.015</b>	<b>0.004</b>	28	0.009	0.003	28	0.015	0.004
0046	440	14.6	<b>399</b>	0.192	0.028	97	<b>0.082</b>	<b>0.017</b>	33	1.387	1.331	440	0.002	0.001
0099	299	47.4	<b>190</b>	<b>0.709</b>	0.697	104	0.862	<b>0.402</b>	243	1.096	0.618	278	0.015	0.005
1001	285	43.9	<b>251</b>	<b>0.767</b>	<b>0.276</b>	241	2.943	0.86	280	0.085	0.053	284	3.747	1.963
0231	296	42.2	<b>246</b>	<b>0.065</b>	0.014	214	0.133	<b>0.011</b>	284	0.022	0.011	290	0.062	0.008
0411	299	29.9	<b>273</b>	<b>0.02</b>	<b>0.009</b>	188	1.65	0.338	288	0.013	0.007	290	0.026	0.012
0377	295	27.5	<b>210</b>	<b>0.043</b>	0.014	162	0.044	<b>0.01</b>	279	0.158	0.022	288	0.042	0.008
0102	299	25.8	<b>284</b>	<b>0.059</b>	<b>0.007</b>	255	0.619	0.032	155	3.47	2.859	267	0.017	0.004
0147	298	24.6	<b>207</b>	<b>0.325</b>	<b>0.088</b>	197	0.581	0.097	251	0.215	0.041	295	0.195	0.018
0148	287	24.6	197	<b>0.122</b>	<b>0.024</b>	<b>206</b>	0.172	0.028	249	0.119	0.023	277	2.004	0.581
0446	298	22.1	<b>288</b>	<b>0.065</b>	<b>0.013</b>	283	0.26	0.021	294	0.148	0.006	298	0.014	0.005
0022	297	21.2	<b>274</b>	<b>0.039</b>	<b>0.011</b>	241	0.233	0.025	289	0.654	0.008	290	0.015	0.008
0327	298	21	271	<b>0.096</b>	<b>0.006</b>	<b>281</b>	0.443	0.022	294	0.008	0.003	295	0.316	0.091
0015	284	20.6	<b>215</b>	<b>0.167</b>	<b>0.021</b>	142	0.914	0.105	185	0.984	0.053	282	0.039	0.006
0455	298	19.8	<b>293</b>	<b>0.105</b>	<b>0.01</b>	<b>293</b>	0.17	0.014	298	0.109	0.012	298	0.03	0.008
0496	297	19.2	<b>281</b>	<b>0.055</b>	<b>0.006</b>	<b>281</b>	0.322	0.197	293	0.045	0.009	295	0.038	0.007
1589	299	17.4	<b>290</b>	<b>0.037</b>	<b>0.003</b>	284	0.207	0.008	296	0.069	0.004	299	0.006	0.002
0012	299	16.3	287	<b>0.058</b>	<b>0.023</b>	<b>291</b>	0.475	0.131	294	0.044	0.013	295	0.052	0.014
0104	284	16.2	193	<b>0.038</b>	<b>0.009</b>	<b>220</b>	2.254	0.568	200	0.07	0.019	283	0.189	0.047
0019	299	15.4	250	<b>0.008</b>	<b>0.004</b>	<b>267</b>	0.411	0.128	296	0.254	0.097	298	0.005	0.001
0063	293	14.5	<b>262</b>	<b>0.083</b>	<b>0.013</b>	<b>262</b>	0.583	0.057	275	0.301	0.009	292	0.028	0.003
0130	285	14.4	<b>192</b>	<b>0.024</b>	<b>0.005</b>	<b>192</b>	0.114	0.03	282	0.179	0.041	285	0.077	0.016
0080	284	12.9	<b>139</b>	<b>0.097</b>	<b>0.01</b>	137	0.418	0.012	163	0.173	0.011	283	0.804	0.754
0240	298	11.9	<b>275</b>	0.422	0.09	274	<b>0.411</b>	<b>0.064</b>	296	0.168	0.006	298	0.023	0.006
0007	290	11.7	172	<b>0.053</b>	<b>0.01</b>	<b>260</b>	2.305	1.432	286	0.301	0.053	290	0.008	0.003

**Table 2:** MegaDepth experiment. The table shows the mean and median camera location error. (Above the middle rule are Group 1 scenes with <1000 images; below are Group 2 scenes with >1000 images, subsampled to 300 for testing.)

Scene	$N_c$	Outliers%	Ours		ESFM		ESFM*		Colmap	
			$N_r$	Mean	$N_r$	Mean	$N_r$	Mean	$N_r$	Mean
0205	910	51.8	<b>386</b>	<b>0.6</b>	70	0.83	633	0.8	782	0.57
0238	522	44.6	<b>283</b>	0.62	76	<b>0.48</b>	512	0.65	515	0.73
0060	528	41.6	<b>503</b>	<b>0.64</b>	303	0.97	524	0.59	525	0.67
0197	870	40.7	<b>667</b>	<b>0.67</b>	281	0.74	825	0.58	847	0.66
0094	763	40.1	<b>537</b>	<b>0.82</b>	93	0.95	643	0.87	743	0.75
0265	571	38.8	<b>346</b>	<b>0.62</b>	270	1.04	559	0.59	560	0.68
0083	635	31.3	<b>596</b>	<b>0.68</b>	568	0.71	556	0.81	633	0.69
0076	558	30.5	<b>524</b>	<b>0.73</b>	454	0.78	547	0.71	550	0.82
0185	368	30	<b>350</b>	<b>0.73</b>	261	<b>0.73</b>	130	1.51	367	0.74
0048	512	24.2	<b>474</b>	<b>0.63</b>	469	0.72	508	0.62	507	0.7
0024	356	23	<b>309</b>	<b>0.78</b>	271	0.91	343	0.71	351	0.77
0223	214	17	<b>204</b>	<b>0.59</b>	191	0.69	211	0.51	214	0.57
5016	28	16.9	<b>28</b>	0.77	<b>28</b>	<b>0.56</b>	28	0.44	28	0.55
0046	440	14.6	<b>399</b>	0.72	97	<b>0.53</b>	33	1.45	440	0.72
<hr/>										
0099	299	47.4	<b>190</b>	0.94	104	<b>0.83</b>	243	1.01	278	0.67
1001	285	43.9	<b>251</b>	1.09	241	<b>0.96</b>	280	0.74	284	1.15
0231	296	42.19	<b>246</b>	0.93	214	<b>0.87</b>	284	0.75	290	0.85
0411	299	29.9	<b>273</b>	<b>0.67</b>	188	0.73	288	0.6	290	0.7
0377	295	27.50	<b>210</b>	0.62	162	<b>0.58</b>	279	0.56	288	0.67
0102	299	25.8	<b>284</b>	<b>0.68</b>	255	0.71	155	1.35	267	0.68
0147	298	24.6	<b>207</b>	<b>0.63</b>	197	<b>0.63</b>	251	0.58	295	0.6
0148	287	24.6	197	0.73	<b>206</b>	<b>0.71</b>	249	0.57	277	0.63
0446	298	22.1	<b>288</b>	<b>0.71</b>	283	0.79	294	0.65	298	0.68
0022	297	21.2	<b>274</b>	<b>0.6</b>	241	0.64	289	0.54	290	0.62
0327	298	21	271	<b>0.85</b>	<b>281</b>	0.87	294	0.66	295	0.74
0015	284	20.6	<b>215</b>	<b>0.56</b>	142	0.65	185	0.67	282	0.6
0455	298	19.8	<b>293</b>	<b>0.73</b>	<b>293</b>	0.78	298	0.66	298	0.73
0496	297	19.2	<b>281</b>	<b>0.6</b>	<b>281</b>	0.61	293	0.55	295	0.62
1589	299	17.4	<b>290</b>	<b>0.58</b>	284	<b>0.58</b>	296	0.52	299	0.56
0012	299	16.3	287	<b>0.55</b>	<b>291</b>	0.56	294	0.54	295	0.6
0104	284	16.2	193	<b>0.81</b>	<b>220</b>	0.86	200	0.67	283	0.72
0019	299	15.4	250	<b>0.62</b>	<b>267</b>	0.7	296	0.61	298	0.66
0063	293	14.5	<b>262</b>	<b>0.68</b>	<b>262</b>	0.75	275	0.59	292	0.65
0130	285	14.4	<b>192</b>	<b>0.8</b>	<b>192</b>	0.88	282	0.68	285	0.76
0080	284	12.9	<b>139</b>	<b>0.77</b>	137	0.8	163	0.69	283	0.67
0240	298	11.9	<b>275</b>	<b>0.54</b>	274	0.58	296	0.53	298	0.6
0007	290	11.7	172	<b>0.63</b>	<b>260</b>	0.68	286	0.54	290	0.59

**Table 3:** Megadepth experiment. The table shows the mean reprojection error (pixels). (Above the middle rule are Group 1 scenes with <1000 images; below are Group 2 scenes with >1000 images, subsampled to 300 for testing.)

Scene	$N_c$	Outliers%	Ours			ESFM			ESFM*			Colmap		
			$N_r$	Mean	Median	$N_r$	Mean	Median	$N_r$	Mean	Median	$N_r$	Mean	Median
Alamo	573	32.6	<b>484</b>	<b>3.662</b>	<b>0.97</b>	457	4.532	0.995	526	3.168	0.347	568	2.166	0.193
Ellis Island	227	25.1	<b>214</b>	<b>0.784</b>	<b>0.302</b>	196	21.131	18.875	220	0.379	0.192	223	0.212	0.124
Madrid Metropolis	333	39.4	<b>244</b>	<b>8.422</b>	<b>4.423</b>	151	19.562	19.849	290	25.247	23.709	323	0.893	0.159
Montreal Notre Dame	448	31.7	<b>419</b>	<b>1.349</b>	<b>0.575</b>	309	10.131	4.421	414	0.163	0.069	447	0.149	0.086
Notre Dame	549	35.6	<b>518</b>	<b>0.778</b>	<b>0.281</b>	487	1.949	0.433	528	0.721	0.298	546	2.652	1
NYC Library	330	33.6	<b>224</b>	<b>3.961</b>	<b>1.478</b>	177	4.417	1.929	301	2.62	1.155	330	0.361	0.14
Piazza del Popolo	336	33.1	<b>249</b>	<b>2.202</b>	<b>0.8</b>	204	10.768	3.199	303	4.314	0.882	334	0.444	0.176
Tower of London	467	27	94	<b>0.672</b>	<b>0.48</b>	<b>196</b>	22.024	13.586	213	13.079	4.526	467	0.546	0.291
Vienna Cathedral	824	31.4	483	<b>0.982</b>	<b>0.381</b>	<b>551</b>	6.519	1.397	536	1.512	0.442	824	1.02	0.349
Yorkminster	432	28.9	<b>331</b>	14.544	<b>4.672</b>	215	<b>10.629</b>	6.149	389	12.628	6.481	419	0.219	0.141

**Table 4:** 1DSFM experiment. The table shows the mean and median camera rotation error (degrees).

Scene	$N_c$	Outliers%	Ours			ESFM			ESFM*			Colmap		
			$N_r$	Mean	Median	$N_r$	Mean	Median	$N_r$	Mean	Median	$N_r$	Mean	Median
Alamo	573	32.6	<b>484</b>	0.689	<b>0.037</b>	457	<b>0.338</b>	0.047	526	0.389	0.016	568	1.197	0.013
Ellis Island	227	25.1	<b>214</b>	<b>0.138</b>	<b>0.035</b>	196	2.091	1.554	220	0.033	0.026	223	0.047	0.022
Madrid Metropolis	333	39.4	<b>244</b>	<b>0.899</b>	<b>0.193</b>	151	1.932	1.641	290	2.655	2.154	323	0.053	0.012
Montreal Notre Dame	448	31.7	<b>419</b>	<b>0.176</b>	<b>0.047</b>	309	1.778	0.79	414	0.023	0.009	447	0.022	0.012
Notre Dame	549	35.6	<b>518</b>	<b>0.186</b>	<b>0.015</b>	487	0.233	0.025	528	0.055	0.012	546	0.216	0.044
NYC Library	330	33.6	<b>224</b>	<b>0.494</b>	<b>0.074</b>	177	0.546	0.102	301	0.226	0.087	330	0.058	0.01
Piazza del Popolo	336	33.1	<b>249</b>	<b>0.194</b>	<b>0.034</b>	204	1.006	0.353	303	0.652	0.052	334	0.042	0.011
Tower of London	467	27	94	<b>0.061</b>	<b>0.012</b>	<b>196</b>	2.226	0.564	213	0.704	0.163	467	0.053	0.02
Vienna Cathedral	824	31.4	483	<b>0.087</b>	<b>0.015</b>	<b>551</b>	0.553	0.046	536	0.076	0.013	824	0.164	0.02
Yorkminster	432	28.9	<b>331</b>	1.492	<b>0.299</b>	215	<b>0.636</b>	0.302	389	1.089	0.265	419	0.028	0.007

**Table 5:** 1DSFM experiment. The table shows the mean and median camera location error.

Scene	$N_c$	Out.	Ours		ESFM		ESFM*		Colmap	
			$N_r$	Mean	$N_r$	Mean	$N_r$	Mean	$N_r$	Mean
Alamo	573	32.6	<b>484</b>	0.94	457	<b>0.86</b>	526	0.82	568	0.92
Ellis Island	227	25.1	<b>214</b>	<b>0.79</b>	196	1.58	220	0.78	223	0.88
Madrid Metropolis	333	39.4	<b>244</b>	<b>0.68</b>	151	0.95	290	1.1	323	0.74
Montreal Notre Dame	448	31.7	<b>419</b>	<b>1.16</b>	309	<b>1.16</b>	414	0.96	447	1.06
Notre Dame	549	35.6	<b>518</b>	1.33	487	<b>1.3</b>	528	1	546	1.12
NYC Library	330	33.6	<b>224</b>	1.09	177	<b>0.73</b>	301	0.94	330	1.08
Piazza del Popolo	336	33.1	<b>249</b>	<b>1.03</b>	204	1.27	303	1.01	334	0.96
Tower of London	467	27	94	<b>0.72</b>	<b>196</b>	0.84	213	0.87	467	0.98
Vienna Cathedral	824	31.4	483	1.15	<b>551</b>	<b>1.1</b>	536	0.93	824	1.06
Yorkminster	432	28.9	<b>331</b>	1.26	215	<b>1.08</b>	389	1.05	419	1.05

**Table 6:** 1DSFM experiment. The table shows the mean reprojection error.

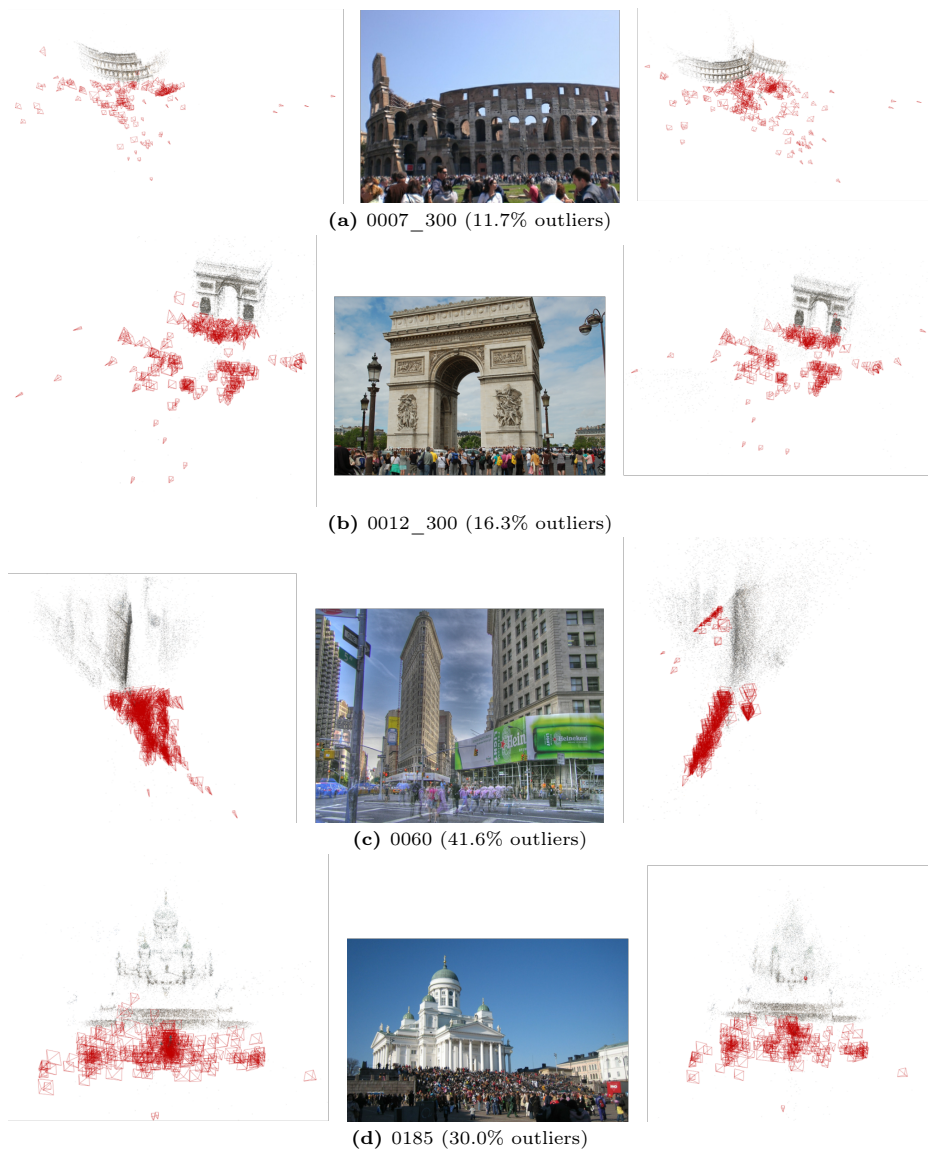


**Fig. 2:** MegaDepth dataset. 3D reconstructions and camera pose estimation. The triplet in each line shows our method reconstruction on the left, one of the input images in the middle, and the reconstruction of ESFM [23] on the right.

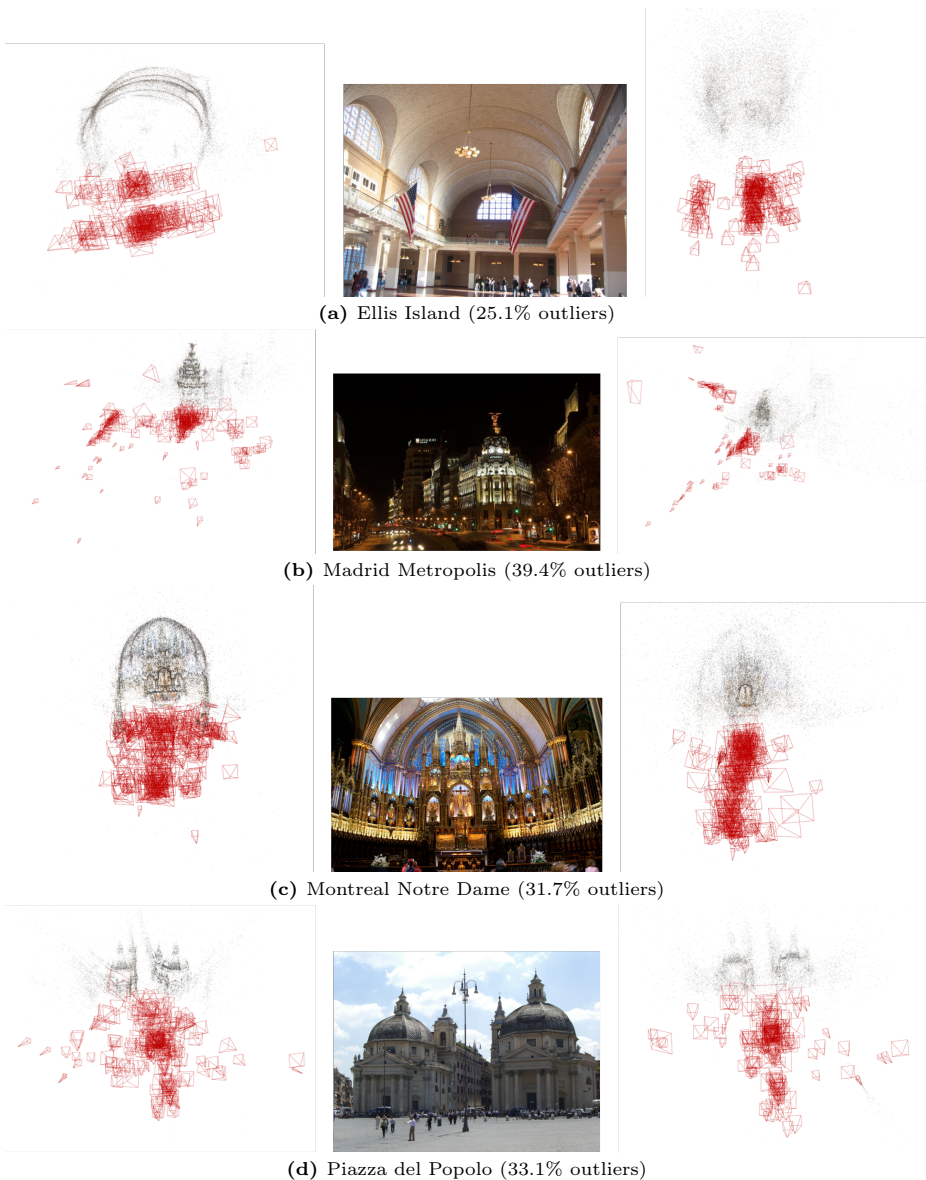


**Fig. 3:** 1DSFM dataset. 3D reconstructions and camera pose estimation. The triplet in each line shows our method reconstruction on the left, one of the input images in the middle, and the reconstruction of ESFM [23] on the right.

## 4.4 Results

Our results for the Megadepth and 1DSFM test scenes are detailed in Tables 2 to 3 and Tables 5 to 6, respectively. For both datasets, we present camera location errors (Tables 2 and 5), camera rotation errors (Tables 1 and 4), and reprojection errors (Tables 3 and 6). Each table lists the number of input images ( $N_c$ ), the fraction of outliers, our results, and comparisons with ESFM on original and cleaned tracks (denoted ESFM\*), as well as COLMAP results using our tracks. For each method, we detail the number of images used and the mean and median errors for camera rotation and location, with reprojection errors reported as means.

It can be seen that our method outperforms ESFM in almost all runs, achieving accurate results that are close to what is obtained with ESFM on clean tracks and with Colmap with our original tracks. This demonstrates the utility of our method in realistic settings.

**Visual results.** Figures 2 and 3 show the 3D reconstructions and camera parameters obtained using our method compared to those obtained with *ESFM* [23]. The comparison clearly demonstrates that our method produces superior 3D reconstructions. A limitation of our method can be observed in Figure 3b, where a significant number of images is excluded from the output due to a large number of false positive predictions (inliers that are predicted as outliers). Addressing this limitation presents an avenue for future research.

**Runtime.** Table 7 compares the runtimes of our method with Colmap. Our approach is significantly faster, though the fine-tuning phase is the most time-consuming part of our pipeline.

Scene	$N_c$	Outliers%	Ours					COLMAP	
			Inference	Fine-tuning	BA	Total (Mins)	$N_r$	Total (Mins)	$N_r$
Alamo	573	32.60%	0.004	674.30	355.57	17.16	484	83.67	568
Ellis Island	227	25.10%	0.004	103.40	66.06	2.82	214	14.89	223
Madrid Metropolis	333	39.40%	0.003	286.80	61.18	5.80	244	25.12	323
Montreal Notre Dame	448	31.70%	0.005	190.62	174.90	6.09	419	35.87	447
Notre Dame	549	35.60%	0.003	1101.75	229.43	22.19	518	72.58	546
NYC Library	330	33.60%	0.004	153.15	88.02	4.02	224	26.56	330
Piazza del Popolo	336	33.10%	0.002	91.60	69.96	2.69	249	9.58	334
Tower of London	467	27.00%	0.003	271.65	84.00	5.93	94	65.03	467
Vienna Cathedral	824	31.40%	0.005	470.35	963.46	23.90	483	98.91	824
Yorkminster	432	29.00%	0.002	270.00	192.52	7.71	331	31.42	419

**Table 7:** Runtime (in seconds, except for Total, in mins) of our proposed method for Euclidean Reconstruction on Various Test Scenes, compared to COLMAP.

**Classification performance.** Table 8 presents various classification metrics to assess the performance of our Outlier Removal module. Our method significantly decreases the percentage of outliers in the point tracks after removing the predicted outliers. However, it suffers from a relatively high number of false positive predictions, where inliers are incorrectly identified as outliers.

Scene	$N_c$	Outliers%	Outliers-after%	Acc.	Prec.	Recall(outliers)	Recall(inliers)	F-score
Alamo	573	32.6%	16.0%	68.6%	51.5%	74.3%	65.8%	60.8%
Ellis Island	227	25.1%	13.9%	64.0%	38.4%	70.4%	61.9%	49.7%
Madrid Metropolis	333	39.4%	27.9%	62.5%	51.7%	62.3%	62.6%	56.5%
Montreal Notre Dame	448	31.7%	18.6%	64.4%	46.4%	70.4%	61.5%	56.0%
Notre Dame	549	35.6%	26.0%	62.3%	48.5%	61.4%	62.8%	54.2%
NYC Library	330	33.6%	15.9%	61.7%	46.5%	81.1%	51.7%	59.1%
Piazza del Popolo	336	33.1%	16.3%	63.8%	47.5%	78.1%	56.7%	59.0%
Tower of London	467	27.0%	15.9%	43.6%	30.3%	85.4%	28.3%	44.8%
Vienna Cathedral	824	31.4%	21.2%	60.8%	42.2%	65.8%	58.5%	51.5%
Yorkminster	432	29.0%	18.7%	56.8%	37.5%	71.8%	50.6%	49.3%

**Table 8:** Classification performance, we show various classification metrics to assess the performance of our Outlier Removal module.

## 5 Conclusion

We present a robust solver based on permutation equivariant architecture for the structure from motion problem. Our proposed method can cope with a point track tensor contaminated with many outliers. In addition, we modified the bundle adjustment module to make it robust enough to handle classification errors. Our method achieves high accuracy while reducing the time significantly compared to classical methods. However, our method suffers from limitations we will address in future work. Among the limitations of the technique are that it often fails to consider the entire set of input images and also struggles with a very high outlier ratio.

## Acknowledgments

Research at the Weizmann Institute was partially supported by the Israel Science Foundation, grant No. 1639/19, by the Israeli Council for Higher Education (CHE) via the Weizmann Data Science Research Center, by the MBZUAI-WIS Joint Program for Artificial Intelligence Research and from the Estates of Tully and Michele Plesser and the Anita James Rosen and Harry Schutzman Foundations.

## References

1. Agarwal, S., Furukawa, Y., Snavely, N., Simon, I., Curless, B., Seitz, S.M., Szeliski, R.: Building rome in a day. *Communications of the ACM* **54**(10), 105–112 (2011)
2. Agarwal, S., Mierle, K., Others: Ceres solver. <http://ceres-solver.org>
3. Arnold, E., Wynn, J., Vicente, S., Garcia-Hernando, G., Monszpart, Á., Prisacariu, V.A., Turmukhambetov, D., Brachmann, E.: Map-free visual relocalization: Metric pose relative to a single image. In: *ECCV* (2022)
4. Brynte, L., Iglesias, J.P., Olsson, C., Kahl, F.: Learning structure-from-motion with graph attention networks. *arXiv preprint arXiv:2308.15984* (2023)
5. Cai, R., Hariharan, B., Snavely, N., Averbuch-Elor, H.: Extreme rotation estimation using dense correlation volumes. In: *Proceedings of the IEEE/CVF Conference on Computer Vision and Pattern Recognition*. pp. 14566–14575 (2021)
6. Chen, X., Liu, J., Zhao, H., Zhou, G., Zhang, Y.Q.: Nerrf: 3d reconstruction and view synthesis for transparent and specular objects with neural refractive-reflective fields. *arXiv preprint arXiv:2309.13039* (2023)
7. Chen, Z., Li, J., Li, Q., Yang, B., Dong, Z.: Deepaat: Deep automated aerial triangulation for fast uav-based mapping (2024)
8. DeTone, D., Malisiewicz, T., Rabinovich, A.: Superpoint: Self-supervised interest point detection and description. In: *Proceedings of the IEEE conference on computer vision and pattern recognition workshops*. pp. 224–236 (2018)
9. Fischler, M.A., Bolles, R.C.: Random sample consensus: a paradigm for model fitting with applications to image analysis and automated cartography. *Communications of the ACM* **24**(6), 381–395 (1981)
10. Hartford, J., Graham, D., Leyton-Brown, K., Ravanbakhsh, S.: Deep models of interactions across sets. In: *International Conference on Machine Learning*. pp. 1909–1918. PMLR (2018)
11. He, X., Sun, J., Wang, Y., Peng, S., Huang, Q., Bao, H., Zhou, X.: Detector-free structure from motion. *arXiv preprint arXiv:2306.15669* (2023)
12. Hong, J.H., Zach, C., Fitzgibbon, A.: Revisiting the variable projection method for separable nonlinear least squares problems. In: *2017 IEEE Conference on Computer Vision and Pattern Recognition (CVPR)*. pp. 5939–5947. IEEE (2017)
13. Kasten, Y., Geifman, A., Galun, M., Basri, R.: Algebraic characterization of essential matrices and their averaging in multiview settings. In: *Proceedings of the IEEE/CVF International Conference on Computer Vision*. pp. 5895–5903 (2019)
14. Khatib, F., Margalit, Y., Galun, M., Basri, R.: Leveraging image matching toward end-to-end relative camera pose regression (2024)
15. Kingma, D.P., Ba, J.: Adam: A method for stochastic optimization. *arXiv preprint arXiv:1412.6980* (2014)
16. Laskar, Z., Melekhov, I., Kalia, S., Kannala, J.: Camera relocalization by computing pairwise relative poses using convolutional neural network. In: *Proceedings of the IEEE International Conference on Computer Vision Workshops*. pp. 929–938 (2017)
17. Li, Z., Snavely, N.: Megadepth: Learning single-view depth prediction from internet photos. In: *Proceedings of the IEEE conference on computer vision and pattern recognition*. pp. 2041–2050 (2018)
18. Lin, A., Zhang, J.Y., Ramanan, D., Tulsiani, S.: Relpose++: Recovering 6d poses from sparse-view observations. *arXiv preprint arXiv:2305.04926* (2023)
19. Lindenberger, P., Sarlin, P.E., Larsson, V., Pollefeys, M.: Pixel-perfect structure-from-motion with featuremetric refinement. In: *Proceedings of the IEEE/CVF international conference on computer vision*. pp. 5987–5997 (2021)

20. Lindenberger, P., Sarlin, P.E., Pollefeys, M.: LightGlue: Local Feature Matching at Light Speed. In: ICCV (2023)
21. Lowe, D.G.: Distinctive image features from scale-invariant keypoints. *International journal of computer vision* **60**(2), 91–110 (2004)
22. Martinec, D., Pajdla, T.: Robust rotation and translation estimation in multiview reconstruction. In: 2007 IEEE Conference on Computer Vision and Pattern Recognition. pp. 1–8. IEEE (2007)
23. Moran, D., Koslowsky, H., Kasten, Y., Maron, H., Galun, M., Basri, R.: Deep permutation equivariant structure from motion. In: Proceedings of the IEEE/CVF International Conference on Computer Vision. pp. 5976–5986 (2021)
24. Oechsle, M., Peng, S., Geiger, A.: Unisurf: Unifying neural implicit surfaces and radiance fields for multi-view reconstruction. In: Proceedings of the IEEE/CVF International Conference on Computer Vision. pp. 5589–5599 (2021)
25. Özyeşil, O., Voroninski, V., Basri, R., Singer, A.: A survey of structure from motion\*. *Acta Numerica* **26**, 305–364 (2017)
26. Paszke, A., Gross, S., Massa, F., Lerer, A., Bradbury, J., Chanan, G., Killeen, T., Lin, Z., Gimelshein, N., Antiga, L., et al.: Pytorch: An imperative style, high-performance deep learning library. *Advances in neural information processing systems* **32** (2019)
27. Reizenstein, J., Shapovalov, R., Henzler, P., Sbordone, L., Labatut, P., Novotny, D.: Common objects in 3d: Large-scale learning and evaluation of real-life 3d category reconstruction. In: Proceedings of the IEEE/CVF International Conference on Computer Vision. pp. 10901–10911 (2021)
28. Rockwell, C., Johnson, J., Fouhey, D.F.: The 8-point algorithm as an inductive bias for relative pose prediction by ViTs. arXiv preprint arXiv:2208.08988 (2022)
29. Sarlin, P.E., DeTone, D., Malisiewicz, T., Rabinovich, A.: SuperGlue: Learning feature matching with graph neural networks. In: CVPR (2020), <https://arxiv.org/abs/1911.11763>
30. Schönberger, J.L., Frahm, J.M.: Structure-from-motion revisited. In: Conference on Computer Vision and Pattern Recognition (CVPR) (2016)
31. Sinha, S., Zhang, J.Y., Tagliasacchi, A., Gilitschenski, I., Lindell, D.B.: Sparsepose: Sparse-view camera pose regression and refinement. In: Proceedings of the IEEE/CVF Conference on Computer Vision and Pattern Recognition. pp. 21349–21359 (2023)
32. Snavely, N., Seitz, S.M., Szeliski, R.: Photo tourism: exploring photo collections in 3d. In: ACM siggraph 2006 papers, pp. 835–846 (2006)
33. Sturm, P., Triggs, B.: A factorization-based algorithm for multi-image projective structure and motion. In: European conference on computer vision. pp. 709–720. Springer (1996)
34. Sun, J., Shen, Z., Wang, Y., Bao, H., Zhou, X.: LoFTR: Detector-free local feature matching with transformers. CVPR (2021)
35. Sun, W., Jiang, W., Trulls, E., Tagliasacchi, A., Yi, K.M.: Acne: Attentive context normalization for robust permutation-equivariant learning. In: Proceedings of the IEEE/CVF conference on computer vision and pattern recognition. pp. 11286–11295 (2020)
36. Wang, J., Rupprecht, C., Novotny, D.: Posediffusion: Solving pose estimation via diffusion-aided bundle adjustment. In: Proceedings of the IEEE/CVF International Conference on Computer Vision. pp. 9773–9783 (2023)
37. Wilson, K., Snavely, N.: Robust global translations with 1dsfm. In: Computer Vision–ECCV 2014: 13th European Conference, Zurich, Switzerland, September 6–12, 2014, Proceedings, Part III 13. pp. 61–75. Springer (2014)

38. Wu, C.: Towards linear-time incremental structure from motion. In: 2013 International Conference on 3D Vision-3DV 2013. pp. 127–134. IEEE (2013)
39. Yariv, L., Gu, J., Kasten, Y., Lipman, Y.: Volume rendering of neural implicit surfaces. *Advances in Neural Information Processing Systems* **34**, 4805–4815 (2021)
40. Yariv, L., Kasten, Y., Moran, D., Galun, M., Atzmon, M., Ronen, B., Lipman, Y.: Multiview neural surface reconstruction by disentangling geometry and appearance. *Advances in Neural Information Processing Systems* **33**, 2492–2502 (2020)
41. Yi, K.M., Trulls, E., Ono, Y., Lepetit, V., Salzmann, M., Fua, P.: Learning to find good correspondences. In: *Proceedings of the IEEE conference on computer vision and pattern recognition*. pp. 2666–2674 (2018)
42. Zhang, J.Y., Lin, A., Kumar, M., Yang, T.H., Ramanan, D., Tulsiani, S.: Cameras as rays: Pose estimation via ray diffusion. In: *International Conference on Learning Representations (ICLR)* (2024)
43. Zhang, J.Y., Ramanan, D., Tulsiani, S.: Relpose: Predicting probabilistic relative rotation for single objects in the wild. In: *European Conference on Computer Vision*. pp. 592–611. Springer (2022)
44. Zhang, J., Sun, D., Luo, Z., Yao, A., Zhou, L., Shen, T., Chen, Y., Quan, L., Liao, H.: Learning two-view correspondences and geometry using order-aware network. In: *Proceedings of the IEEE/CVF international conference on computer vision*. pp. 5845–5854 (2019)
45. Zhao, C., Ge, Y., Zhu, F., Zhao, R., Li, H., Salzmann, M.: Progressive correspondence pruning by consensus learning. In: *Proceedings of the IEEE/CVF International Conference on Computer Vision*. pp. 6464–6473 (2021)

## Appendix

### A Implementation details

**Our code and preprocessed point tracks data will be made publicly available.**

**Framework.** Our method was trained and evaluated on NVIDIA A40 GPUs. We used PyTorch [26] as the deep learning framework and the ADAM optimizer [15] with normalized gradients.

**Training.** During training, for each epoch, we processed all training scenes sequentially. For each scene, we randomly selected a subset of 10%-20% of the images in the scene. We used a validation set for early stopping. More specifically, we selected the checkpoint with the minimal reprojection error after Bundle Adjustment. The validation and test sets were evaluated by using the complete point tracks matrix. The training time of our model on the Megadepth dataset took roughly 16 hours on a single NVIDIA A40 GPU.

**Architecture details.** We use normalized point tracks  $\mathbf{x}_{ij}$ , as inputs to our method which are normalized using the known intrinsic parameters. The shared features encoder  $E$  has 3 layers, each with 256 feature channels and ReLU activation. The camera head  $H_{\text{cams}}$ , 3D point head  $H_{\text{pts}}$ , and the outliers classification head  $H_{\text{outlier}}$ , each have 3 layers with 256 channels. After each layer in  $E$  we normalize its features by subtracting their mean.

**Hyper-parameter search.** We tried different implementation hyper-parameters including (1) learning rates  $\in \{1e-2, 1e-3, 1e-4\}$ , (2) network width  $\in \{128, 256, 512\}$  for the encoder  $E$  and the heads, (3) number of layers  $\in \{2, 3, 4, 5\}$  in these networks, and (4) threshold for outlier removal  $\in \{0.4, 0.5, 0.6, 0.7\}$ .

**Bundle adjustment** For the bundle adjustment, we employed the Ceres Solver’s implementation of bundle adjustment [2] with the Huber loss to enhance robustness (with parameter 0.1). In each bundle adjustment round, we limited the number of iterations to 300 or until convergence, whichever occurred first.

### B Constructing point tracks

Our preprocessing step for constructing the point tracks is as follows:

1. Extracting SIFT [21] features for all the images.
2. Applying exhaustive pair-wise RANSAC [9] matching for all image pairs.
3. Chaining each sequence of two-view matches for creating a point track.

We discard a 3D point and its track if it is viewed in less than 3 cameras, or if it includes an inconsistent cycle i.e. we detect two key points in the same image for the same point track.

The above preprocess, defines a valid point track structure for our architecture. We next define the inliers/outliers labeling process which assumes that every training scene has an associated COLMAP [30] reconstruction:

1. For each track within our point track set:
  - (a) Identify the corresponding track in COLMAP’s reconstruction output
  - (b) For every keypoint in the track:
    - Label the keypoint as an outlier if it does not appear in the corresponding COLMAP track ; otherwise, label it as an inlier.
2. Remove keypoints labeled as outliers from the point tracks.
3. Triangulate the 3D points from the cleaned point tracks using the ground truth camera poses, obtained from COLMAP.
4. Calculate the reprojection error for the triangulated 3D points across the entire point tracks, including the ones labeled initially as outliers.
5. Assign an inlier label to each keypoint whose reprojection error is below 4 pixels; keypoints exceeding this threshold are classified as outliers.